This article has been accepted for publication in a future issue of this journal, but has not been fully edited. Content may change prior to final publication. Citation information: DOI 10.1109/ACCESS.2019.2901357, IEEE Access

Digital Object Identifier

STLFM Signal Based Adaptive Synchronization for Underwater Acoustic Communications

FEI YUAN[1], ZHENYU JIA[1], JIANGHUI LI[2], EN CHENG[1]
[1]Key Laboratory of Underwater Acoustic Communication and Marine Information Technology, Xiamen University, Xiamen, China
[2]Institute of Sound and Vibration Research, University of Southampton, Southampton, United Kingdom

Corresponding author: Jianghui LI.

This work is supported by the National Natural Science Foundation of China (61471308,61571377,61771412) and the Fundamental Research Funds for the Central Universities (20720180068).

ABSTRACT In underwater acoustic communications (UAC), signal synchronization plays a key role in the performance. It is usually performed using a known preamble transmitted prior to the data. However, the underwater acoustic (UWA) channel is characterized as time-varying and frequency-varying, which makes the preamble fluctuated as well as the transmitted data. Thus, it contains uncertainty to set a constant threshold for synchronization by using information (e.g., Doppler shift) extracted from the preamble. In this work, we propose an adaptive scheme for UAC synchronization. The scheme uses the symmetrical triangular linear frequency modulation (STLFM) signal to design a Fractional Fourier Transform (FrFT) based detection algorithm. It establishes the frame synchronization by detecting the deviation of the two energy peaks which usually emerge in their "optimal" FrFT domain in pairs. Instead of detecting the absolute peaks, the proposed method performs an initial synchronization and a precise correction based on the relative positional relationship and amplitude attenuation of the two peaks, which makes full use of the two peaks of the STLFM signal in the FRFT domain. The effectiveness of the scheme has been verified by simulations and field works. The results suggest that it is able to peak the time-varying signal amplitude for each frame in UWA channels. Besides, the proposed scheme performs better accuracy and stability in the frame synchronization compared to the traditional LFM method, which is shown as three times less detection error and five to ten times dropping of mean square error (MSE).

INDEX TERMS STLFM (Symmetrical Triangular Linear Frequency Modulation), FrFT (Fractional Fourier Transform), underwater acoustic communication, frame synchronization

I. INTRODUCTION

UNDERWATER acoustic channel is characterized as time-varying and frequency-varying, which distorts the communication signal, especially in extreme environments [1]–[5]. For obtaining good performance of the underwater acoustic communications (UAC), a synchronization frame is usually used in the transmitted packet, known as a preamble. The preamble transmitted prior to the information data is often designed to be easily detected by the receiver [6]. Sequences with good auto-correlation or cross-correlation properties ensures the ability for the preamble to establish the synchronization.

In UAC, bi-phase sequences, such as Barker sequences and M-sequences, are widely used in the preamble for frame synchronization. However, there are some limitations of using the bi-phase sequence, especially in a channel with low signal-to-noise ratio (SNR). To achieve good performance, wide chip duration and long sequence are usually required, which increase the risk of the time selective fading. Besides, the bi-phase sequence is usually modulated by single frequency carrier (sinusoidal or cosinusoidal type). However, the single frequency carrier signals are easily distorted due to frequency selective fading, and further reduce the performance of the frame synchronization [5]–[7].

To overcome these limitations, better signals and sequences structures have been investigated. Sun et al. [8] proposed a synchronization scheme based on binary offset carrier (BOC) modulated signal with no interference windows. The method has sharper auto-correlation peaks compared to the traditional Binary Phase Shift Keying (BPSK)-modulated

bi-phase sequence. Jamshidi [9] presented Direct Sequence Spread Spectrum (DSSS) based multiple pseudo-random sequences to optimize signal from multi-path in the channel and proposed a simple inter-symbol interference (ISI) reduction algorithm to alleviate the ISI effect. He et al. [10] proposed a multi-channel time-frequency domain equalization method for pseudo-random sequences based Single Carrier Frequency-domain Equalization (SC-FDE), which includes a multi-channel frequency domain equalizer followed by a low order multi-channel adaptive time domain decision feedback equalizer (DFE). Su [11] and Yan [12] uses 'chaos' to spread the spectrum. Zhang et al. [7] modulated M-sequences on two orthogonal carriers, in which one is used as a reference sequence and the other is shifted relative to the reference. These methods focus on the performance improvement using the sequences structure.

Apart from the sequences mentioned above, chirp signal also spread spectrum to improve the anti-noise performance [13]. Matched filters are used to obtain the auto-correlation peaks, by which the peaks can be captured directly and are used to process the frequency selective fading. This scheme eliminates the pseudo-random sequences capture and simplifies the synchronization in UWA channels. Further, chirp signals have good toleration for frequency-selective fading and Doppler shift, which make them widely used in the channel estimation. The anti-noise performance of the chirp signal depends on its time-bandwidth product, while the synchronization accuracy relates to its ambiguity function. The synchronization signals in UAC based on LFM and LFM-like signals have been widely studied and achieved good performence [13].

In recent years, new schemes such as the Hyperbolic frequency modulated (HFM) signals, which have good tolerance to the Doppler, have been presented [14], [15]. Symmetrical triangular LFM (STLFM) (Figure 1) is one type of LFM-like signals. It has been used to replace the traditional single slope LFM signal (sawtooth wave) in the study of low probability of intercept (LPI) radar for years [16]. It contains two parts of single slope LFM, which are the positive part and the negative part. They rise linearly to a certain value during the first half of the cycle, and then linearly decreases to the starting point in the second half. Because of this special structure, the STLFM signal can improve the performance of communication systems in the condition of low SNR and fading channels, which makes it widely used in radars with low interception probability. Literature [16]–[18] have shown that the 3 dB blur map area of the STLFM signals is significantly reduced compared to that of the LFM signals, which indicates that the STLFM signal has better time-frequency resolution and is more suitable for low SNR channels. STLFM signal has also been reported to be used as the synchronization in underwater acoustical channel, but it is regarded as two independent LFM signals, its symmetry feature has not been taken into account [19].

Researchers have proposed methods to combine the signals for designing robust structure and determine the exact arrival time of the synchronization. Sharif et al. [20] used Linear Frequency Modulation (LFM) signal as the preamble and postamble for each data package, such that the receiver can estimate the change of the waveform duration. This method estimates the average Doppler scale for the whole data package. It requires a whole data package as the buffer before data demodulation, which prevents the real-time online processing of the receiver. Choi et al. [21] proposed an adaptive serial search acquisition scheme, in which the detection threshold is adaptively scaled by the instantaneous received power in a fast-varying channel. The instantaneous received signal power is estimated for each correlation interval prior to pseudo-random sequences correlation and is used to scale a fixed reference as detection threshold. The scheme significantly reduces acquisition time compared to conventional non-adaptive schemes under Rayleigh fading and pulsed Gaussian noise jamming. Mason et al. [6] proposed a method for detection, synchronization and Doppler scale estimation for UAC using orthogonal frequency-division multiplex (OFDM) waveforms. By transmitting two identical OFDM symbols together with a cyclic prefix, the receiver can use the bank of parallel self-correlator for synchronization, which does not require channel information for synchronization. This method realizes synchronization setting by measuring the bottoms of two peaks and avoids the traditional setting of the absolute threshold of synchronization.

By using the simple LFM-like signals as the synchronization, the anti-noise performance can be achieved and the frequency selective fading and Doppler effect can be overcome. Thus, better signal design and frame structure can make the LFM-like synchronization robust in the UAC channels with low SNR and serious fading. The above method ignores the relationship of LFM signals in LFM-like signals and cannot fully utilize the performance of LFM-like signals in low SNR and frequency selective fading channels. In this paper, an STLFM signal based adaptive synchronization for UAC is proposed. The STLFM is regarded as a special combination of the LFM signals. It is transformed into the FrFT domain, which has symmetrical peaks emerging in their "optimal" points in pair. Thus, we proposed an algorithm to acquire the synchronization by tracking the optima peaks in twins adaptively. The simulation and experimental results show that the proposed synchronization method significantly outperforms traditional methods used for comparison.

The paper is organized as follows. Section II introduces the basic model of STLFM system and the features of STLFM in the FRFT domain. Section III describes the adaptive synchronization scheme which comprises the awaken and the acquisition stages. Section IV presents the performance analysis about the proposed synchronization method in the UAC channel. Section V compares the proposed scheme with the various traditional schemes using simulation and experimental data, and Section VI completes the paper with concluding remarks.

This article has been accepted for publication in a future issue of this journal, but has not been fully edited. Content may change prior to final publication. Citation information: DOI 10.1109/ACCESS.2019.2901357, IEEE Access

II. STFLM SIGNAL AND FRFT

This section describes the structure of the Symmetrical triangular LFM (STLFM) signal and the STLFM in the Fractional Fourier Transform (FrFT) domain.

A. STLFM SIGNAL

The STLFM signal can be regarded as the time-shifted combination of two LFM signals with opposite slopes. LFM signals which are mutually conjugate in a period T and are equivalent to the up-chirp and down-chirp signals in the baseband.

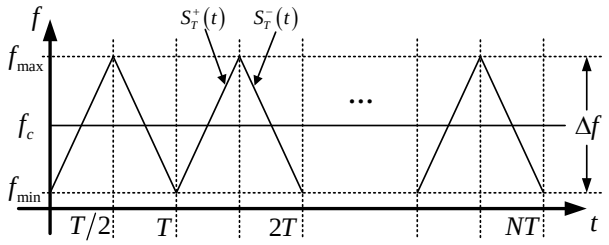

FIGURE 1. N copies of the STLFM Signals.

Figure 1 shows N copies of the STLFM signals marked as $T, 2T, \ldots, NT$. For each period, the STLFM signal consists of two LFM signals with symmetrical slopes. The LFM signal with a positive slope is marked as $S_T^+(t)$ in the first half period ($[0, T/2]$), while the negative slope LFM is marked as $S_T^-(t)$ in the left half ($[T/2, T]$). The $S_T^+(t)$ and the $S_T^-(t)$ are given by:

$$S_T^+(t) = A\exp\{j2\pi[(f_c - \frac{\mu T}{4})t + \frac{\mu t^2}{2}] + j\phi_1\}, \quad (1)$$

$$S_T^-(t) = A\exp\{j2\pi[(f_c + \frac{\mu T}{4})(t - \frac{T}{2}) + \frac{\mu(t - \frac{T}{2})^2}{2}] + j\phi_2\}. \quad (2)$$

where $f_c = (f_{max} + f_{min})/2$, and it is the operative center frequency, μ is the modulation slope, and $\mu = 2B/T$, B is the bandwidth, and $B = f_{max} - f_{min}$, ϕ_1 and ϕ_2 are the initial phases, and $\phi_2 = \pi f_c T + \phi_1$.

In the UAC system, frequency selective fading suffered from the multi-path [3], [22], [23] and the Doppler shift [2], [24] resulted by the relative movement, can be detected by using the synchronization signal. Often, ambiguity function (AF) is used as a metric to judge the accuracy of the synchronization [18]. Here we denote the received signal as $x(t)$:

$$x(t) = s(t) + n(t), \quad (3)$$

where $s(t)$ is the transmitted signal (LFM or STLFM) and $n(t)$ is the noise signal. The AF can be expressed as:

$$\chi(\tau, \varepsilon) = \int_{-\infty}^{+\infty} x(t)x^*(t+\tau)e^{j2\pi\varepsilon t}dt, \quad (4)$$

where τ is the time delay, and ε is the Doppler shift [5].

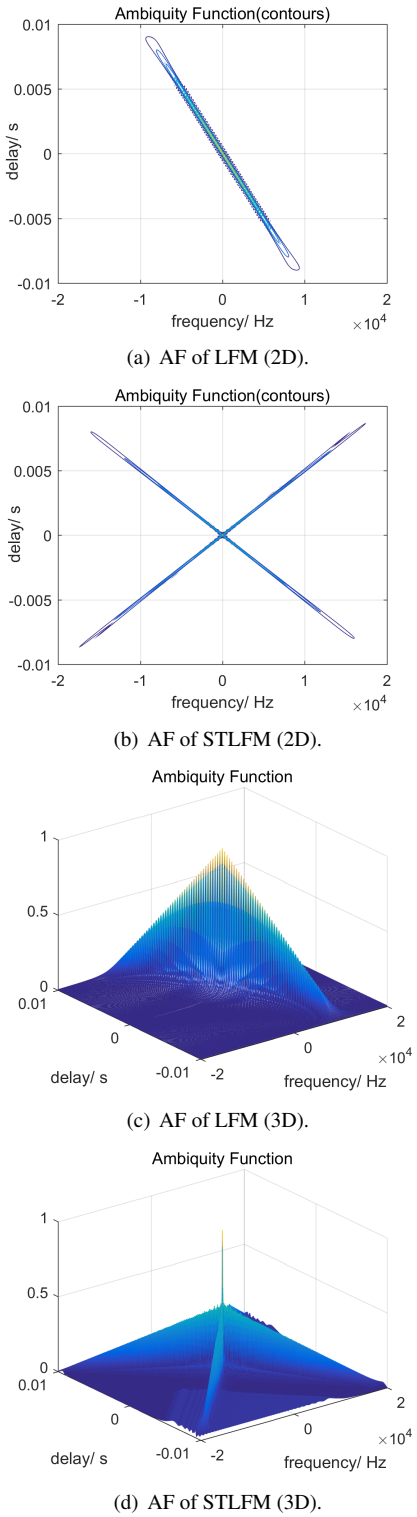

(a) AF of LFM (2D).

(b) AF of STLFM (2D).

(c) AF of LFM (3D).

(d) AF of STLFM (3D).

FIGURE 2. Relation between Ambiguity Functions of LFM and STLFM.

Let the frequency range of both the LFM and STLFM be 20 kHz to 30 kHz, and the duration of them be 5 ms.

Figure 2(a) and Figure 2(b) show the two-dimension (2D) AF results. It is a straight line passing through the origin one with the single-slope LFM signal, while there are two

straight lines passing through the origin with the STLFM signal. Figure 2(c) and Figure 2(d) show that the peak of the STLFM is much sharper than that of the LFM. Thus it is concluded that the STLFM signal is more suitable to act as the preamble for synchronization than the LFM signal.

B. STLFM IN THE FRFT DOMAIN

Matching correlation is widely used in processing the LFM-like signal including STLFM. It obtains the correlation peaks in the time-domain and conducts accurate synchronization acquisition. However, it requires true prior information of the received signal, which is usually sensitive to phase changes. The amplitude, phase, and frequency of a signal are often distorted after traveling through the UWA channel, which affects the matching correlation in the detection. The accuracy of the matching correlation is often determined by parameter settings such as the detection window and the decision threshold, which usually leads to missed detection or misjudgment. To solve these problems, Time-Frequency (S-T) analysis is usually applied in the detection, from which the principal parameters of the signal could be obtained to achieve the synchronization estimation.

Three types of S-T estimation methods for LFM-like synchronization signals have been presented. Cohen method [25] performs good results on detecting the single component of LFM signals. However, its performance drops seriously in the multi-components detection for the reason of serious cross-term interference emerging. In order to overcome cross-interference, Radon-Wigner & Radon-Ambiguity methods [26] convert the problem of the multi-components detection into peak searching, but they need high computational resources. Fractional Fourier Transform is an outstanding S-T method in dealing with the LFM-like signals. It focuses the power in the FrFT domain [27], [28] and does not introduce cross-interference. As an extension of the Fourier Transform, FrFT also possesses a fast calculation which reduces the computational complexity and makes it suitable for LFM-like signals detection. The FrFT of the received signal $x(t)$ can be expressed as:

$$X_p(u) = \int_{-\infty}^{+\infty} K_p(t,u)x(t)dt. \tag{5}$$

The $K_p(t,u)$ is expressed as:

$$K_p(t,u) = \begin{cases} A_\alpha \exp[j\pi(u^2\cot\alpha \\ \quad -2ut\csc\alpha + t^2\cot\alpha)], & \alpha \neq n\pi, \\ \delta(t-u), & \alpha = 2n\pi, \\ \delta(t+u), & \alpha = (2n\pm 1)\pi, \end{cases} \tag{6}$$

where the coefficient $A_\alpha = \sqrt{1-j\cot\alpha}$, the transformation angle $\alpha = p\pi/2$, the order $p \neq 2n$, and n is an integer.

The traditional computation of the FrFT is complicated compared to the Fast Fourier Transform (FFT). Simplified FrFT algorithm proposed by Chen [29] help to reduce the complexity significantly, which is given by:

$$X_\alpha(f') = \int_{-\infty}^{+\infty} \exp[j(\pi\cot\alpha)t^2 - j2\pi f't]x(t)dt, \tag{7}$$

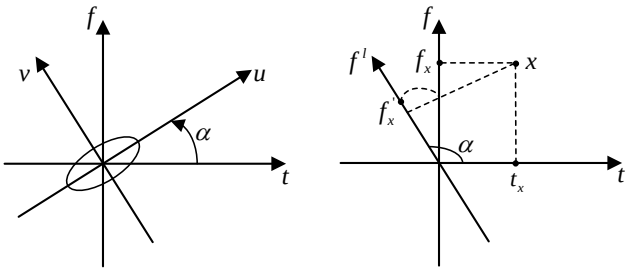

(a) FrFT. (b) CFrFT.

FIGURE 3. Comparison of FrFT and CFrFT.

where $\alpha \neq (0,\pi)$. The discrete form of it can be expressed as:

$$X_\alpha(k) = \sum_{n=0}^{N-1} x(\frac{n}{\sqrt{N}})\exp[j(\pi\cot\alpha)(\frac{n}{\sqrt{N}})^2 - j\frac{2\pi}{N}nk] \tag{8}$$

where N is the number of sampling points. Compared to the traditional FrFT (Figure 3), the CFrFT only rotates the frequency axis of the time-frequency plane, and the conversion result is the same as that of the FrFT, but the complexity is reduced significantly. The discrete computation requires only one multiplication of LFM signal and one FFT operation, which facilitates the real-time synchronization.

Assume there is no time delay or frequency shift, the positions of the peaks in the FrFT domain are given by:

$$u_1 = (f_c - \frac{\mu T}{4})\sin\alpha, \tag{9}$$

and

$$u_2 = (f_c + \frac{3\mu T}{4})\sin(-\alpha), \tag{10}$$

where α is the transformation angle of the up-chirp part of the STLFM, f_c is the operative center frequency. The positions of the peaks are related to f_c and α. By subtracting Eq.(9) from Eq.(10), we obtain the distance and the position of the symmetry axis between the two peaks:

$$|u_2 - u_1| = (2f_c + \frac{\mu T}{2})\sin\alpha = 2f_{max}\sin\alpha, \tag{11}$$

$$\frac{|u_2 + u_1|}{2} = \frac{\mu T}{2}\sin\alpha = B\sin\alpha, \tag{12}$$

The center frequency of the down-chirp part of STLFM is $f_c - \mu T/4$, and in the FrFT the frequency at the start of the transform window is considered as the equivalent center frequency $f_c + 3\mu T/4$. The distance between two peaks is related to f_{max} and α. Considering the time delay and frequency shift in the UWA channel, the positions of the peaks in the FrFT domain u_{1r} and u_{2r} are given by:

$$u_{1r} = u_1 - \tau\cos\alpha - \varepsilon\sin\alpha, \tag{13}$$

$$u_{2r} = u_2 - \tau\cos(-\alpha) - \varepsilon\sin(-\alpha), \tag{14}$$

where τ is the time delay, ε is the frequency shift. From Eq.(13) and Eq.(14), we can obtain the distance and the

position of the symmetry axis between the two peaks affected by multipath and frequency shift:

$$|u_{2r} - u_{1r}| = |u_2 - u_1 - 2\varepsilon \sin\alpha| = 2(f_{max} - \varepsilon)\sin\alpha, \quad (15)$$

$$\frac{|u_{2r} + u_{1r}|}{2} = \frac{|u_2 + u_1 - 2\tau\cos\alpha|}{2} = B\sin\alpha - \tau\cos\alpha, \quad (16)$$

From Eq.(15), we can see that the time delay will cause the position of the symmetry axis to change, based on this, we can obtain the delay of the current synchronization window according to the offset of the symmetry axis of the peaks in the FrFT domain, thereby achieve the synchronization acquisition. From Eq.(16), we know that the frequency shift will change the spacing between the two peaks, based on this, we can estimate the Doppler factor, and then adjust the optimal FrFT order.

III. ADAPTIVE SYNCHRONIZATION SCHEME

Figure 4 shows the architecture of the synchronous system. First, there is a wake-up module (Section III-A) that keeps running state, which is used to detect the arrival or not of the synchronization signal. When the wake-up module detects the arrival of the synchronization signal, the synchronization capture module is started (Section III-B). The synchronous acquisition module consists of two parts. The initial synchronization is first performed according to the relative positional relationship between the two peaks in the FrFT domain, and then the finer correction is performed according to the double-peak amplitude attenuation in the FrFT domain after the initial synchronization. In the wake-up module, the combination of the matched filter and the FrFT detector effectively reduces the probability of false alarms, while the synchronization acquisition module makes full use of the properties of the two peaks of the STLFM signal in the FrFT domain rather than the detection of absolute peaks.

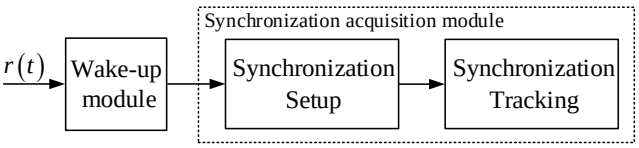

FIGURE 4. system framework.

A. SYNCHRONIZATION AWAKEN

Fluctuation is usually presented in the synchronization signal transmitted through the UAC channel. It brings difficulties to the threshold setting for the synchronization detection. Too high or too low of the threshold would increase the detection error. To reduce the error, we propose an adaptive synchronization scheme that contains the awaken stage and the acquisition stage as shown in Figure 5.

In the awakening stage, the module searches potential signal that acts as the synchronization and then starts the system to confirm its authenticity. Traditional methods for the awaken are usually based on a constant threshold [30]. However, the noise and interference in the channel make it difficult to achieve adaptive wake-up using the constant threshold for the preamble. The proposed method uses the orthogonality of LFM-like signal to separate the true signal and the noise.

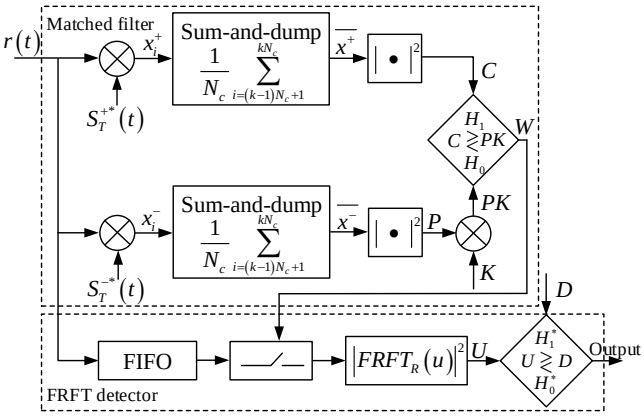

FIGURE 5. Framework of the Awaken Module. The received signal $r(t)$ enters the matched filter and the FrFT detector respectively.

In Figure 5, the input signal enters three branches, by which the awaken module is divided into two parts, each of them is marked as a dashed box. The first part is a matched filter, and the second part is an FrFT detector. In the matched filter part, the input signal enters two matching branches respectively (marked as up branch and down branch). The matched filter in the up branch matches the first half period ($[0, T/2]$) to detect the STLFM positive slope LFM signal segment $S_T^+(t)$. In the down branch, the matched filter matches the second half period ($[T/2, T]$) to detect the STLFM negative slope LFM signal segment $S_T^-(t)$. For the wake-up module, the up and down branches are orthogonally matched with each other. In the FrFT detector part, the input signal enters in a First-In First-Out (FIFO) at the beginning and waits for the output W of the matched filter. Once the output of the matched filter reaches the threshold, the FrFT detector will be switched on, and the signal stored in the FIFO is then transformed. In the FrFT domain, since the peak value of the signal reaches the threshold, the synchronization system will be woken up.

The combination of the FrFT detector and the matched filter is used to minimize the probability of false alarms. If a matched filter is used alone, affected by noise, the output may also exceed the threshold, causing false alarms. And If only the FrFT detector is used, When the received interference signal happens to be an LFM-like signal that the optimal FrFT order is the same with the wake-up signal, the peak value in the FrFT domain also exceeds the threshold, resulting in a false alarm. In addition, the capture of the arrival time of the signal is also an important issue. Matched filtering can be equivalent using a correlator, and correlation is the best reception of the signal in the time domain, which

This article has been accepted for publication in a future issue of this journal, but has not been fully edited. Content may change prior to final publication. Citation information: DOI 10.1109/ACCESS.2019.2901357, IEEE Access

is more suitable for wake-up and can lay the foundation for subsequent precise synchronization.

Compared to traditional methods using single-slope LFM signal for the wake-up module, the proposed method uses two different matched filters in two branches, which helps to overcome and eliminate the threshold fluctuation caused by the impact noise. Two real-time outputs $\mathrm{Up}_{\mathrm{out}}(t)$ and $\mathrm{Dn}_{\mathrm{out}}(t)$ can be obtained by using sliding correlation operation. Let

$$r(t) = f\big(s(t-\tau_0) + w(t)\big), \tag{17}$$

where $f(\cdot)$ is the transfer function of the channel, $s(t)$ is the STLFM signal, $w(t)$ is an independent zero mean white Gaussian random process with variance of δ_n^2 modeling the additive noise, and τ_0 [s] is the time delay at the moment when the waveform is transmitted. The matched outputs of the two branches are given by:

$$\mathrm{Up}_{\mathrm{out}}(t) = \int_{-T/2}^{T/2} r(t) S_T^{+*}(t) dt, \tag{18}$$

and

$$\mathrm{Dn}_{\mathrm{out}}(t) = \int_{-T/2}^{T/2} r(t) S_T^{-*}(t) dt. \tag{19}$$

We consider a binary hypothesis that denotes the received signal matched the local copy as H_1, and denotes the miss-matched as H_0. Then the hypothesis test is performed by comparing the correlation value C to the power-scaled threshold PK, where K is a fixed reference-detection threshold. If the C is higher than the PK, H_1 is declared, vice versa. The probability of C being higher than PK is given as follows:

$$P_r\{C > PK\} = P_r\{\mathrm{Up}_{\mathrm{out}}(t) > K \cdot \mathrm{Dn}_{\mathrm{out}}(t)\}, \tag{20}$$

and

$$P_r\{C < PK\} = 1 - P_r\{C > PK\}. \tag{21}$$

The probability of leakage detection of chirp binary orthogonal keying (BOK) modulation on White Gaussian Noise (WGN) channel is given by [28]:

$$P_f(\rho, \gamma) = Q(a, b) - \frac{1}{2} \exp\big(\frac{-(a^2+b^2)}{2}\big) I_0(ab), \tag{22}$$

where $Q(x)$ is Q function, γ represents the SNR (Eb/N0) of the received signal,

$$a = \sqrt{\frac{\gamma}{2}(1 - \sqrt{1-|\rho|^2})}, b = \sqrt{\frac{\gamma}{2}(1 - \sqrt{1+|\rho|^2})}, \tag{23}$$

and

$$|\rho| = \frac{1}{\sqrt{BT}} \sqrt{\big(C(\frac{\pi}{2} BT_c)\big)^2 + \big(S(\frac{\pi}{2} BT_c)\big)^2}. \tag{24}$$

From Eq.(24), we can see that the larger the BT_c, the smaller the $|\rho|$, which results in a smaller false detection probability. Thus, the increasing of BT_c improves the detection performance [31]. Figure 6(a) and 6(b) illustrates the relationship of $|\rho|$, BT_c and Eb/N0 according to the Eq.(22)-Eq.(24). If the $|\rho|$ of the two chirp signals equal to 0.1, they are regarded as nearly orthogonal. While if the BT_c excesses 40, the correlation coefficient $|\rho|$ is close to 0.1 and keeps stable. The results reveal that the BT_c can be set large enough to keep the orthogonality between the positive and negative slope of the STLFM signal.

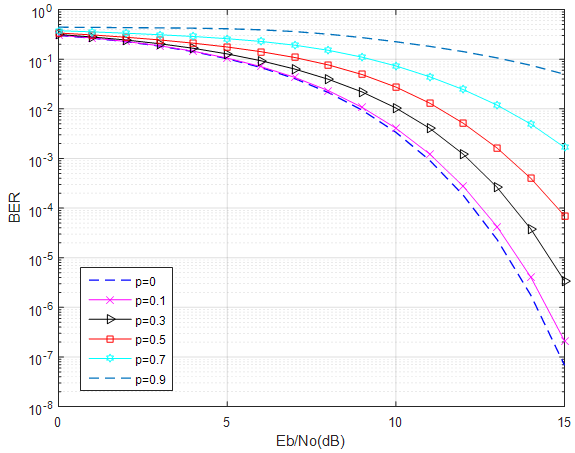

(a) SNR (Eb/N0) and $|\rho|$.

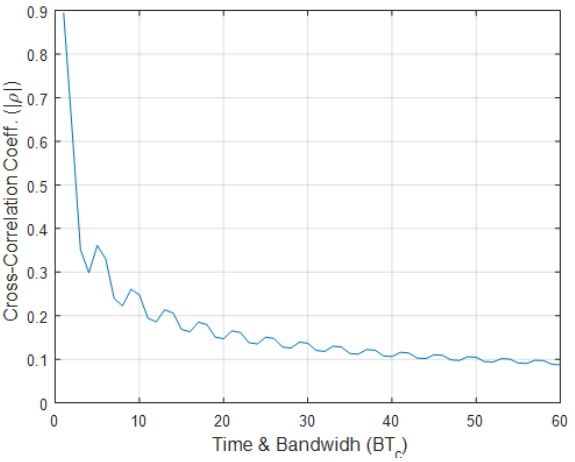

(b) $|\rho|$ and BT_c.

FIGURE 6. The Design of wake-up function.

After awakening the first stage, the system starts to analyze the signal in the FrFT domain for further confirming on the time-frequency characteristics to avoid false alarm, noted as the rechecking stage. In this stage, once the frequency of chirp matches the order of FrFT, the chirp signal exhibits obvious impulse peak characteristic in p-order FrFT domain [32]. If the received signal is not an STLFM signal, even though the energy condition for synchronization wake-up is satisfied, it will not form energy aggregation in the FrFT domain. Thus we can use FrFT to eliminate the false alarm signal.

In the FrFT detector part, we consider another binary hypothesis test. It denotes the case when the peak value of the signal in the FrFT domain reaching the threshold as H_1^*, while the opposite case is denoted as H_0^*. By comparing the peak value U in the FrFT domain to the threshold D, the

This article has been accepted for publication in a future issue of this journal, but has not been fully edited. Content may change prior to final publication. Citation information: DOI 10.1109/ACCESS.2019.2901357, IEEE Access

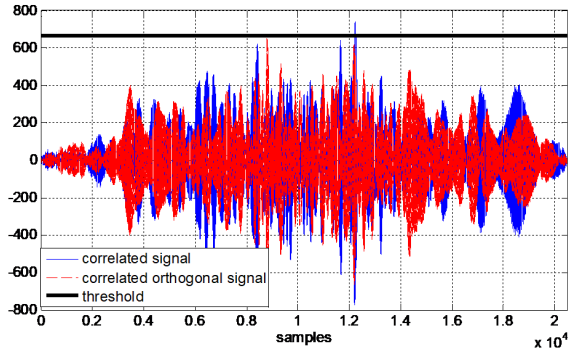

(a) output of the matched filter.

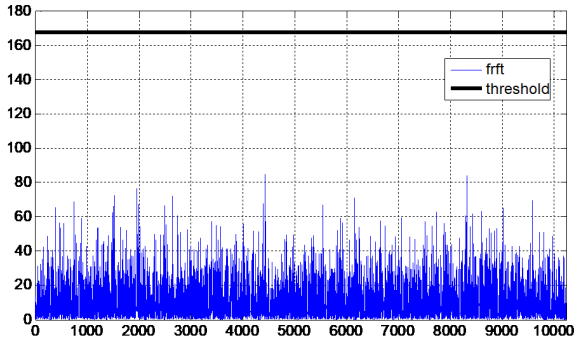

(b) output of the FrFT detector.

FIGURE 7. Wake-up signal is not arrived.

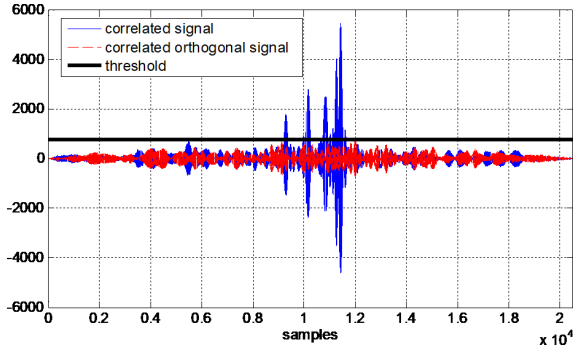

(a) output of the matched filter.

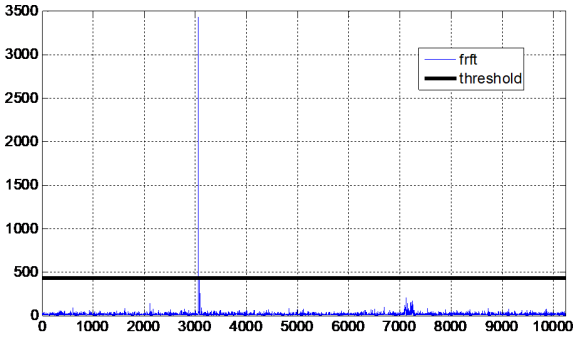

(b) output of the FrFT detector.

FIGURE 8. Wake-up signal is arrived.

hypothesis testing is performed. If the U is higher than D, H_1^* is declared, vice versa. The probability of U being higher than D is given by:

$$P_r\{U > D\} = P_r\{S(k)_{\max} > D\}, \tag{25}$$

and

$$P_f\{U < D\} = 1 - P_r\{U > D\}, \tag{26}$$

where $S(k)$ is the p-order FrFT transformation of the received signal $s(t)$, the $S(k)_{\max}$ is the maximum value of $S(k)$, and the order p is the optimal order for FrFT of the local signal. Once the FrFT detector outputs H_1^*, the detector confirms that the received signal is indeed a wake-up signal rather than a false alarm, at which point the synchronization system is woken up.

In Figure 7(a), the correlated signal (blue) is the up branch of the matched filter (Figure 5) while the correlated orthogonal signal (red) is the down branch and the black line is the threshold. Due to the disturbance, the noise peak sometimes exceeds the dynamic threshold and causes false alarms. At the rechecking stage, the maximun value in the FrFT domain is still below the threshold as shown in Figure 7(b). Thus the false alarm is eliminated and the system is still sleeping [33]. Another example is shown in Figure 8(a) the output of the matched filter activated the FrFT detector as the wake-up signal arrives. In this case, the rechecking in the FrFT domain shown in Figure 8(b) confirms the fact that the use of a matched filter and an FrFT detector can effectively eliminate the effects of false alarm signals [34].

B. SYNCHRONIZATION ACQUISITION

In the above scheme, the positive/negative slope section of the STLFM signal $\left(S_T^+(t)/S_T^-(t)\right)$ is structurally compatible with the traditional LFM signal wakeup design, and both of them are correlated in the time domain. After being awakened, the system switches to the synchronization acquisition stage, which is based on the analysis in the FrFT domain. The system contains two functional modules, which are the "Synchronous Setup based on Symmetry Axis Detection" and the "Synchronous Tracking based on Peak Difference Detection".

Figure 9 shows the synchronous acquisition. The synchronization window is ahead of the received signal, such that the attenuation of the signal in the direct path is minimized. In this case, the start point of the FrFT window is located at the left end of the signal's start point. Then, the symmetry axis is corrected to pull the signal and the FrFT transform window closer to each other. This avoids peaks attenuation of the signal in the direct path and further reduces the computational complexity of the subsequent synchronization processing. After that, the impact of the Doppler shift needs to be compensated for better outputs of peaks. Finally, the FrFT transformation of the original signal is performed after full synchronization. The transformation angle is the expanded angle α.

This article has been accepted for publication in a future issue of this journal, but has not been fully edited. Content may change prior to final publication. Citation information: DOI 10.1109/ACCESS.2019.2901357, IEEE Access

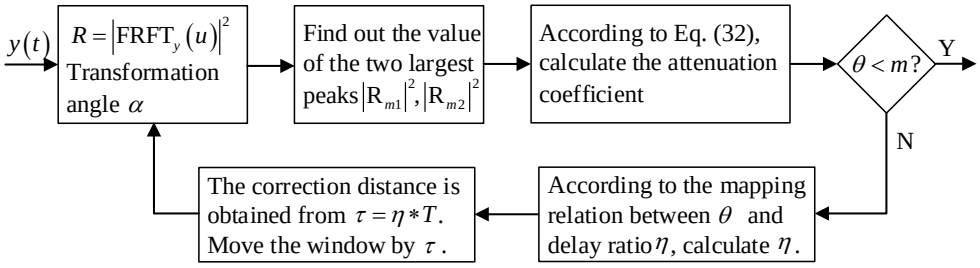

FIGURE 10. Flow diagram of Synchronization tracking.

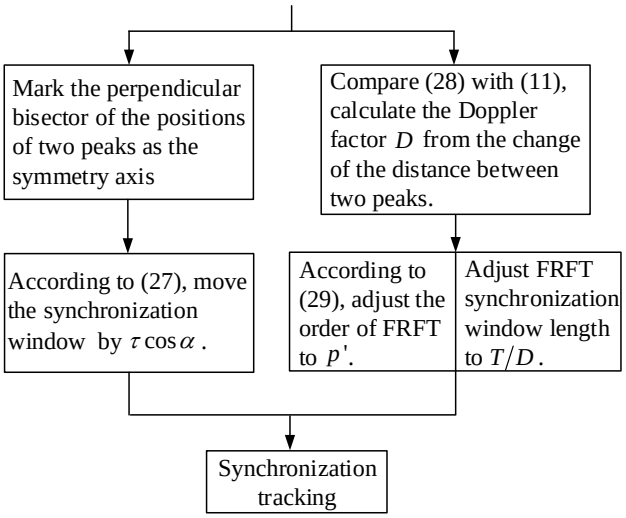

FIGURE 9. Process of synchronization acquisition.

According to Eq.(13) and Eq.(14), the positions of the symmetry axis of the two peaks are given by:

$$(u_{2r}+u_{1r})/2=(u_2+u_1)/2-\tau\cos\alpha, \tag{27}$$

where u_{1r} and u_{2r} represent the positions of the two peaks affected by the time delay. The symmetry axis moves only from the time delay because the Doppler shifts on the up-chirp and down-chirp parts are compensated. By subtracting the symmetry axis obtained from the initial FrFT result of the received signal and the original symmetry axis parameters, the time delay $\tau\cos\alpha$ is obtained, and the location of synchronization window is adjusted.

Assuming that the Doppler factor is D, the maximum frequency becomes Df_{max} at this time. Since the Doppler spread has limited effect in the optimal order of FrFT, by using the original order for FrFT, energy focusing will still appear in the FrFT domain. After the Doppler shift, the spacing of the two peaks in the FrFT domain is given by:

$$|u_{2\varepsilon}-u_{1\varepsilon}|=2Df_{max}\sin\alpha, \tag{28}$$

where $u_{1\varepsilon}$ and $u_{2\varepsilon}$ are the Doppler shifted positions of the two peaks. Combining Eq.(28) with Eq.(11), we can calculate the Doppler shift, and adjust the optimal FrFT order according to

$$p'=-\frac{2}{\pi}\operatorname{arccot}(D^2\mu). \tag{29}$$

At the same time, the length of the FrFT window is adjusted to the duration of received STLFM signal T/D. After correcting the symmetry axis, there will still be an energy overflow due to the slight deviations in the synchronization position, and the two peaks in the FrFT domain are different in amplitude. The synchronous tracking loop can be used to accurately track these signals. The synchronization tracking loop is a closed loop, aiming at locking the amplitude difference of the two peaks below the pre-set threshold. The synchronization deviation is estimated by the amplitude difference of the two peaks, which does not need to set an absolute threshold. Figure 10 shows the diagram of the synchronization tracking.

After synchronizing and correcting the symmetry axis of the signal, the optimal order of FrFT is updated. Then, perform FrFT on the signal with the updated order p', and analyse the value of the two peaks $|R_{m1}|^2$ and $|R_{m2}|^2$. Let u be the position of the peak, and the relation between delay ratio η and attenuation coefficient θ is given by:

$$\begin{aligned}\theta&=1-\frac{\arg\min\{|R_{m1}|^2,|R_{m2}|^2\}}{\arg\max\{|R_{m1}|^2,|R_{m2}|^2\}}\\&=1-(1-|\eta|^2)\operatorname{sinc}^2(\pi uT^2\eta(1-|\eta|)).\end{aligned} \tag{30}$$

Then, by establishing the mapping table, the delay ratio η is obtained, which determines the movement distance τ of the synchronization window. The synchronization window is moved by τ, and the steps above are repeated for the next synchronization tracking loop until the θ is smaller than the pre-set threshold m (see Section IV-A). This means that the difference between the amplitudes of the two peaks is controlled within an acceptable range. At that time, the amplitudes of the two peaks are close to each other, which means a successful synchronization.

IV. PERFORMANCE ANALYSIS

This section analyzes the anti-noise, anti-multipath, and anti-Doppler performance of the proposed method.

This article has been accepted for publication in a future issue of this journal, but has not been fully edited. Content may change prior to final publication. Citation information: DOI 10.1109/ACCESS.2019.2901357, IEEE Access

A. ANTI-NOISE PERFORMANCE

The synchronization acquisition requires comparison of the peaks in the FrFT domain, but the amplitudes of the peaks will be affected at low SNR. Assume that a discrete signal $x(k)$ is superimposed with a random noise, thus the peaks in the FrFT domain appear random fluctuations and have a certain mean square error (MSE). To avoid detection missing, we set an attenuation threshold m based on the relative fluctuation of the peaks to provide a flexible range for detection, then the derivation is expressed as [18]:

$$\frac{\mathcal{V}\left(|X_{p_0}(u_0)+N_{p_0}(u_0)|^2\right)}{|X_{p_0}(u_0)|^2} = \frac{2|A_{\alpha_0}|^2A^2}{(2f_{max})^2\mathrm{SNR}_{\mathrm{in}}^2}+\frac{2|A_{\alpha_0}|^2A^2}{(2f_{max})^2\mathrm{SNR}_{\mathrm{in}}}(2N+1), \tag{31}$$

and

$$m = k\sqrt{\frac{2|A_{\alpha_0}|^2A^2}{(2f_{max})^2\mathrm{SNR}_{\mathrm{in}}^2}+\frac{2|A_{\alpha_0}|^2A^2}{(2f_{max})^2\mathrm{SNR}_{\mathrm{in}}}(2N+1)}, \tag{32}$$

where $\mathcal{V}(\cdot)$ denotes the variance, $N_{p_0}(u_0)$ is the noise amplitude at the signal peaks, N is the data length, the input $\mathrm{SNR}_{\mathrm{in}} = A^2/(\sigma_n^2)$, $A_{\alpha_0} = \sqrt{1-j\cot\alpha_0}$, and k is a coefficient adjusted depending on the actual situation. Eq.(31) shows the relation between fluctuation level and the $\mathrm{SNR}_{\mathrm{in}}$. It is seen that when the sampling rate and parameters of the signal are determined, the $\mathrm{SNR}_{\mathrm{in}}$ becomes a key factor affecting the relationship between the amplitudes of the peaks.

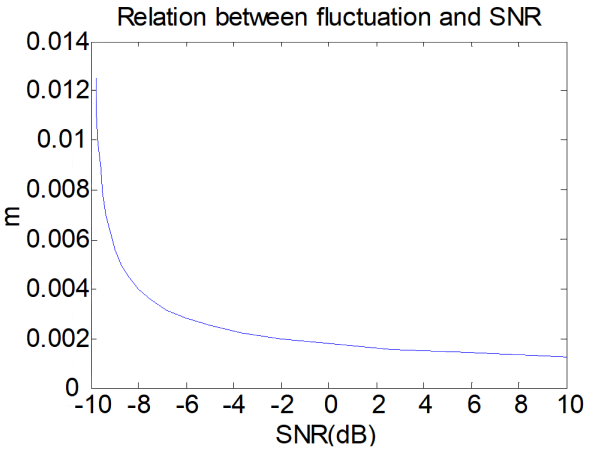

FIGURE 11. Relation between SNR and the Attenuation threshold.

Figure 11 shows the relation between SNR and the threshold m, where f_{max} = 30 kHz, N = 10000, k = 1, A = 1, and $A_{\alpha_0} = \sqrt{1-j}$. As the SNR increases, the attenuation threshold we set will decrease. When the SNR is in the range of -10 to -8, the attenuation threshold drops rapidly. When the SNR is greater than -8, the variation of the attenuation coefficient tends to be gentle. This is because, when the SNR is low, the amplitudes fluctuate greatly. Increasing the attenuation threshold helps to avoid missing detection. Moreover, the requirement for the synchronization tracking based on the amplitude attenuation of the two peaks is also appropriately relaxed. According to Eq. (12), since the positions of the symmetry axis of the peaks are independent with the amplitudes, the correction of the symmetry axis is the key step under the condition of low SNR, so that the system still has a good performance. When the SNR increases, the attenuation decreases, and the relationship between the two peaks' amplitudes tends to be stable. At this time, the setting of the attenuation threshold is also reduced and remains stable, so that the synchronization tracking based on the attenuation of the peaks can further improve the synchronization accuracy in the condition of high SNR.

B. ANTI-MULTIPATH PERFORMANCE ANALYSIS

The two parts of the STLFM signal have the same duration, bandwidth, and frequency. FrFT transforms an STLFM signal with a transformation window of equal length to the signal. When the positions of the window and the signal completely coincide, there will be two peaks of the same value in the FrFT domain. If there is a deviation between the positions of the window and the signal, the peaks positions may change, and the value of the two peaks will also be changed. Inaccurate signal synchronization indicates certain delay, and the FrFT transformation is sensitive to it. Take an LFM signal as an example:

$$f(t) = A\exp(j2\pi f_0 t + j\pi\mu t^2 + j\phi). \tag{33}$$

When there is no time delay, FrFT transforms the signal in $[-T/2, T/2]$, and let the $\alpha = \mathrm{arccot}(-\mu)$ and $u = f_0\sin\alpha$, and u is the position of the peak in the FrFT domain. Then the value of the peak is given by:

$$|F_\alpha(u)|^2\big|_{\alpha=\mathrm{arccot}(-\mu),u=f_0\sin\alpha} = \frac{A^2T^2}{|\sin\alpha|}. \tag{34}$$

When there is a time delay τ, the range of the LFM signal for the FrFT transformation is considered as $[-T/2+\tau, T/2]$. Then, the value of the peak is given by:

$$|F_\alpha(u)|^2\big|_{\alpha=\mathrm{arccot}(-\mu),u=f_0\sin\alpha} = \frac{A^2(T-|\tau|)^2}{|\sin\alpha|}\,\mathrm{sinc}^2\left(\pi\mu\tau(T-|\tau|)\right). \tag{35}$$

The attenuation coefficient is obtained by the subtraction of Eq.(34) and Eq.(35):

$$\theta = 1-(1-|\eta|)^2\,\mathrm{sinc}^2\left(\pi\mu T^2\eta(1-|\eta|)\right), \tag{36}$$

where η is the delay ratio, and $\eta = \tau/T$. The mapping relation Eq.(30) is based on Eq.(36). It can be seen that as the delay ratio increases, the amplitude of the peak decays fast. Therefore, when the synchronization position of the STLFM signal slightly deviates, the amplitudes of the two peaks in the FrFT domain will also be different. When the synchronization position is inaccurate or the synchronization window falls on the multi-path signal component, the amplitudes of the direct path signal may be even smaller than the signal from other paths. However, this only occurs when

the synchronization window lags behind the direct path signal component. The sensitivity of the amplitude attenuation results in the direct path signal submerged by the multipath signal. When the synchronization window is ahead of the direct path signal component, the direct path signal is always closest to the starting point of the synchronization window and will not be submerged. The synchronization methods mentioned above use the direct path signal as the analysis object. Therefore, after the system wakes up, it is necessary to ensure that the synchronization window is slightly ahead of the STLFM signal. The above analysis is based on the premise that the signal from the first arrival path has the largest amplitude among received signals from all paths, which is the condition for the best performance of the proposed algorithm.

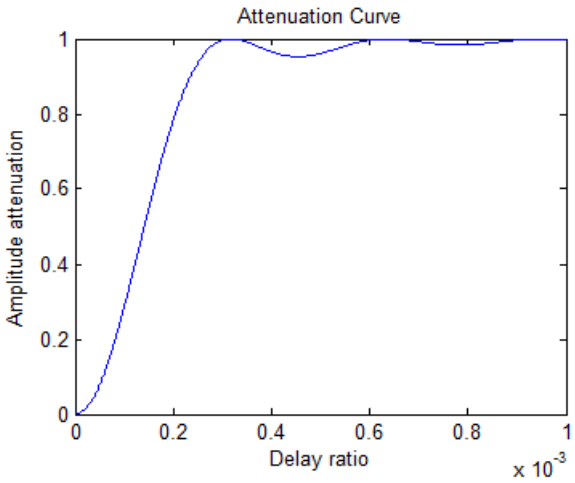

FIGURE 12. Relation between delay ratio and amplitude attenuation.

Figure 12 shows the relation between delay ratio and amplitude attenuation, where the bandwidth B = 10 kHz, and T = 0.1 s. As the time delay of the multipath component increases, the attenuation of the peak is more severe. When the delay ratio reached 0.3 or more, the peak attenuation coefficient was close to 1. This indicates that not only the positions of the peaks of the multipath components will have an offset (Eq. (27)), but also the amplitudes will be greatly attenuated. Since the initial position of the FrFT window is ahead of the signal position during the synchronization setup phase, it is difficult for the multipath components to interfere with the detection of the peak of the direct path. Moreover, in the case where the multipath parameters of the channel remain unchanged, the longer the duration of the signal, the better the anti-multipath performance.

C. ANTI-DOPPLER PERFORMANCE ANALYSIS

1) Effect of Doppler Shift on FrFT order.

Normally, after the synchronization establishment, the optimal transformation angle and optimal order of the signal along with Doppler spread will be determined. However, for FrFT in the phase of symmetry axis correction, the α is not the optimal transformation angle for the original signal. In order to keep the positions of the two peaks, the transformation angle of the original and received signal in this step should be the same. The original signal is an ideal signal, which is not severely affected by the Doppler spread, thus the peak position u can still be obtained accurately. Due to the Doppler effect, the signal is shrunk or stretched in time-domain, and the frequency also changes. Assume the optimal orders for FrFT of the signals before and after Doppler spreading as p and p', separately. Based on the relation between the Doppler factor and the spacing property of peaks positions, the difference between p and p' is given by:

$$\begin{aligned}\Delta p = p' - p &= -\frac{2}{\pi}\operatorname{arccot}(D^2\mu) + \frac{2}{\pi}\operatorname{arccot}\mu \\ &= -\frac{2}{\pi}\arctan\frac{(D^2-1)\mu}{D^2\mu^2+1},\end{aligned} \tag{37}$$

where $D = 1 + v/c$, v is the relative speed between the receiver and the transmitter, and c is the sound speed in underwater acoustic channel. The Δp is given by:

$$\Delta p = -\frac{2}{\pi}\arctan\frac{(2vc+v^2)\mu}{(v+c)^2\mu^2+c^2}. \tag{38}$$

Assume $\mu = 0.1$, v =10 m/s, according to Eq.(38), the Δp is about -0.00075. Normally, the carriers of the transmitter and the receiver move at a speed of a few meters per second in water. The Δp is in the order of 10^{-4}, which is too small to make a difference to the FrFT transformation. As a result, the peaks in the FrFT domain is still clearly using the original order p, and the symmetry axis correction can still be performed effectively. Synchronization acquisition can be optimized by the simple correction procedure for Doppler spread mentioned in Section III-A.

After the FrFT of the signal using the original optimal order, based on the spacing of the peaks positions, the Doppler factor D can be estimated according to the Eq.(28), and then the optimal order is adjusted according to the Eq.(29). Then, the signal is analyzed in the FrFT Domain with order adjusting, and the synchronization acquisition based on the symmetry axes of the two peaks is re-executed, further reducing the error of the initial synchronization. In literature [35], the FrFT with order adjusting is used to analyze the LFM signal to estimate the parameters including multipath and Doppler factor of the channel, and the performance is greatly improved compared with the method without order adjusting.

2) Effect of Doppler Shift on Peak Amplitude

Set the received LFM signal as:

$$g(t) = A\exp\left(j2\pi(f_0+f_d)t + j\pi\mu t^2 + j\phi\right), \tag{39}$$

This article has been accepted for publication in a future issue of this journal, but has not been fully edited. Content may change prior to final publication. Citation information: DOI 10.1109/ACCESS.2019.2901357, IEEE Access

where f_d is the Doppler shift. If there is no time delay, the FrFT of the signal in the interval of $[-T/2, T/2]$ is given by:

$$G_\alpha(u) = A\sqrt{1-j\cot(\alpha)} \times \int_{-T/2}^{T/2} e^{j\pi(t^2\cot(\alpha)-2ut\csc(\alpha)+u^2\cot(\alpha))} e^{j\pi(\mu t^2+2(f_0+f_d)t+j\phi)} dt. \tag{40}$$

The amplitude of the peak in FrFT domain is given by:

$$|G_\alpha(u)|\big|_{\alpha=\operatorname{arccot}(-\mu),u=f_0\sin\alpha} = \frac{4A^2\sin^2(\pi T f_d)}{(2\pi f_d)^2|\sin\alpha|}, \tag{41}$$

Compared with Eq.(34), and define γ as the frequency shift ratio, and $\gamma = f_d/(1/T)$, and the attenuation coefficient θ_d can be obtained by dividing the values before and after frequency shift:

$$\theta_d = \frac{4\sin^2(\pi T f_d)}{(2\pi f_d)^2 T^2} = \operatorname{sinc}^2\gamma, \tag{42}$$

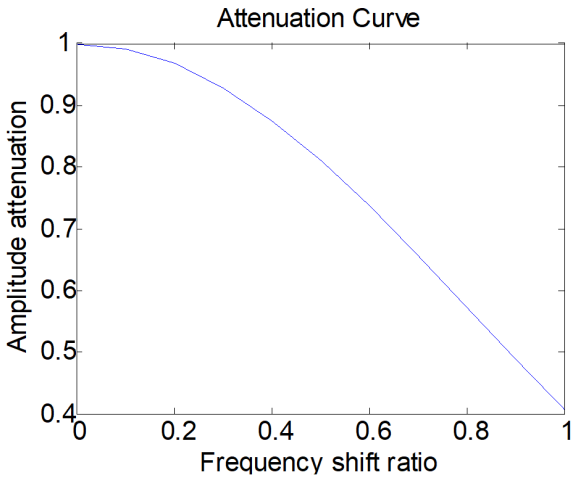

FIGURE 13. Relation between the frequency shift ratio and the amplitude attenuation.

Figure 13 shows the relation between the frequency shift ratio and the amplitude attenuation. As the frequency shift ratio increases, the amplitude of the peak is attenuated more severely. However, in reality, the frequency shift ratio will remain in a low range, so the attenuation of the amplitude does not affect the normal peak detection. Therefore, the main problem caused by Doppler shift is the movement of the peaks positions of the received signal in the FrFT domain, which has been solved by the correction of symmetry axis and the order adjusting.

V. STATISTICAL RESULTS AND DISCUSSION

Traditional synchronization method uses an LFM signal as the synchronization signal, and the synchronization error is determined by the change of peak position in the FrFT domain. In literature [36], the author proposed a synchronization method based on the HFM signal with good anti-Doppler performance. Here we compare the LFM, HFM and STLFM synchronization in the performance using simulation and experimental data. In the simulation, the proposed STLFM and the contrasted LFM and HFM method are all tested for 500 times using the Bellhop ray-trace program [37]. The synchronization error obtained by each test is calculated using the histogram and the error distribution probability. The histogram (Figures 15 & 19) emphasizes the stability of the synchronization of the two methods, and the error distribution probability (Figures 16 & 20) can show the performance difference of the three methods.

A. SIMULATION ON DUAL DISPERSIVE CHANNEL

Table 1 shows the parameters of the UWA channel. The bandwidth of the LFM, HFM, and STLFM signals are from 20 kHz to 30 kHz. The duration of them are 100 ms and the sampling rate is set to 100 kHz.

Since the real ocean channel is a time-frequency dual dispersive channel, in the simulation, we added a Doppler effect ($v = 10m/s$) to form a dual dispersive channel, and added Gaussian white noise.

TABLE 1. The parameters of the simulation channel using the Bellhop model

Parameter	value
Communication distance	1000 [m]
Depth of transducer	10 [m]
Depth of receiver transducer	15 [m]
Root mean square of surface roughness	2 [m]
acoustic velocity	1530 [m/s]
Absorption coefficient of longitudinal wave	0.5
Depth of water	20 [m]
Seawater density	1021 [kg/m^3]
Silt density	1810 [kg/m^3]
The center frequency of the signal	25000 [kHz]
Number of transmit beams	6

Figure 14(a) shows the Power Spectral Density (PSD) of the received signal, from which we can see that the PSD is affected by the multipath and is no longer smooth, meanwhile, the frequency band also has a certain degree of offset. Figure 14(b) to Figure 14(d) show the three types of possible results in the FrFT domain. In addition to the signal components from the direct path, it is seen that other multi-path signal components are also included. However, these signals are significantly attenuated and do not affect the detection of the peaks. Besides, Figure 14(b) shows that the twin peak equals to each other in the FrFT domain, which means that the synchronization is detected at the perfect time. 1000 points ahead or behind the perfect synchronization time can be seen from the Figure 14(c) and Figure 14(d). The difference between the twin peak illustrates the synchronization offset from the perfect time.

We tested the proposed synchronization algorithm for 500 frames. The synchronization error obtained from each

This article has been accepted for publication in a future issue of this journal, but has not been fully edited. Content may change prior to final publication. Citation information: DOI 10.1109/ACCESS.2019.2901357, IEEE Access

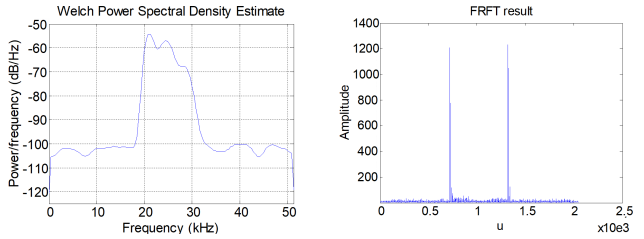

(a) Power Spectral Density (b) Precise point in the perfect time.

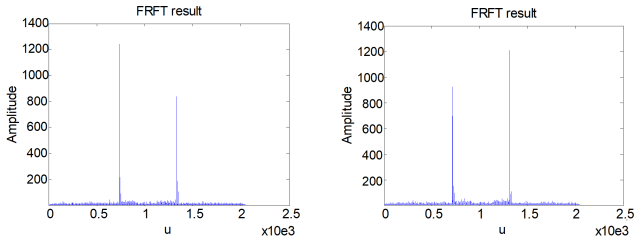

(c) 1000 points ahead the perfect time. (d) 1000 points behind the perfect time.

FIGURE 14. Received signal obtained using Bellhop program and its FrFT results.

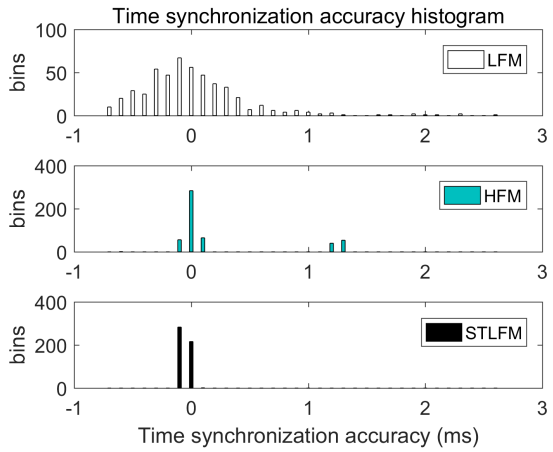

FIGURE 15. Synchronization Error Histogram SNR = -10 dB.

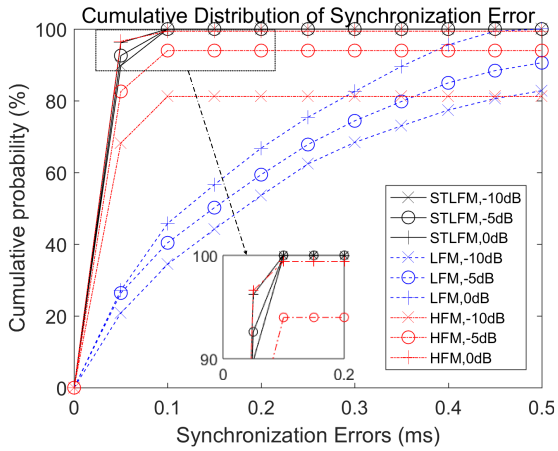

FIGURE 16. Error distribution probability.

test is statistically calculated using the histogram and the error distribution probability, as shown in Figure 15 and Figure 16. In the histogram, the negative and positive axis for time synchronization accuracy respectively indicate that the synchronization time is advanced and delayed. The error distribution probability uses the absolute value of the error regardless of the advance or delay of time. Figure 15 and Figure 16 show that most errors of the proposed method are within a very small range. And almost all of the errors are within 0.1 ms. As a comparison, most of the errors from the LFM synchronization are evenly distributed in the range of 0.8 ms, and the probability of error within 0.1 ms is about only 35%. And the performance of HFM synchronization method is also good, most of the errors are in the range of 0.1 ms, however, due to this method uses a matched filter to achieve synchronization, the anti-multipath performance is poor. As can be seen from Figure 15, some of the errors are around 1.2 ms, and this means that the multipath component of the received signal is synchronized, which leads to a drop in system performance. Because the STLFM method and the LFM method analyze the peaks in the FrFT domain, they have better anti-multipath performance than the HFM method (See Section IV-B), but the FrFT method also affects the synchronization accuracy to some extent, so the error mean of the HFM algorithm is lower. Referring to Figure 12, in the proposed method, if the error is larger than 0.2 ms, even though the amplitude attenuation and delay ratio are not one-to-one mapped, the error can still be further reduced by the correction of the symmetry axis. After several synchronization acquisitions, the error can be within 0.1 ms. Thus, the amplitude attenuation and delay ratio become one-to-one mapped, which can further reduce the error to an even smaller range.

TABLE 2. The error mean and MSE from simulation.

Method	Error Mean [ms]	MSE [ms^2]
STLFM	0.033	2.3×10^{-4}
LFM	0.18	0.017
HFM	0.0181	0.021

Table 2 shows the simulation synchronization error. The error mean is the arithmetic mean of the absolute error values, indicating the accuracy of synchronization. The MSE is the squared average of the distance from each error to the mean, indicating the stability of synchronization. The error mean of the proposed method is five times lower than that from the LFM synchronization, and the MSE of the proposed method is two orders of magnitude lower than that from the LFM method. As for the HFM method, the Error mean is ten times lower than the LFM method, but due to the wrong synchronization of the multipath components, the MSE is much higher than that of the STLFM method.

This article has been accepted for publication in a future issue of this journal, but has not been fully edited. Content may change prior to final publication. Citation information: DOI 10.1109/ACCESS.2019.2901357, IEEE Access

(a) Wu-yuan Bay(Satellite).

(b) Wu-yuan Bay Bridge.

(c) Xiamen Island(Satellite).

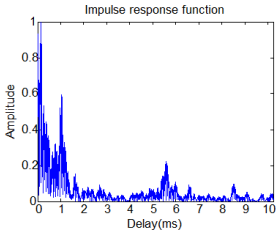

(d) Impulse response function.

FIGURE 17. Field experiment and the channel structure (550 meters).

TABLE 3. The parameters of Wuyuan Bay test channel

Parameter	value
Communication distance	550 [m]
Depth of transducer	5 [m]
Depth of receiver transducer	4 [m]
Depth of water (transmitting end)	7 [m]
Depth of water (receiving end)	6 [m]
The center frequency of the signal	25 [kHz]
Sampling rate of acquisition card	100 [kHz]
Wind speed	3.6 [m/s]
Transducer bandwidth	10 [kHz]
Emissive power	12 [W]

B. EXPERIMENTAL RESULTS

Apart from applying the simulation data, we also use experimental data to verify the effectiveness of the proposed synchronization method. The experiment was conducted in the Wuyuan Bay, Xiamen, China. The transmitter and the receiver were fixed at the Trestle Bridge, and the distance between them was 550 m (Figure 17). Table 3 shows the setting experimental parameters, and the parameters of the signals and Doppler shift are the same as that in Section V-A.

Figure 17(d) shows the measured impulse response of the channel. It is seen that the multi-path components are numerous, and the fading of the channel is more complicated than that in the simulation (Section V-A). The amplitude of the signal from the first path is not the largest, which affects the synchronization performance. Figure 18 shows the received signal from the experimental channel.

In the channel, the power spectrum of the signal is affected, and the frequency selective fading caused by the multi-path effect was complicated. As can be seen from the FrFT results (Figure 18), the amplitudes of the two peaks are different, and

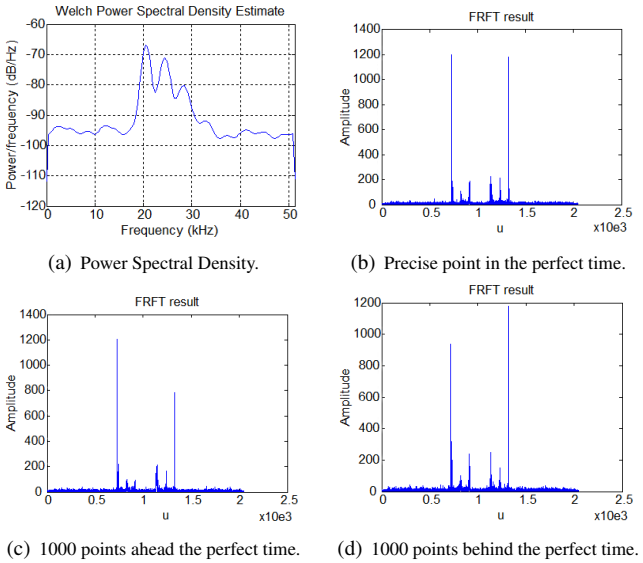

(a) Power Spectral Density. (b) Precise point in the perfect time.

(c) 1000 points ahead the perfect time. (d) 1000 points behind the perfect time.

FIGURE 18. Received signal from the experiment and its FrFT results.

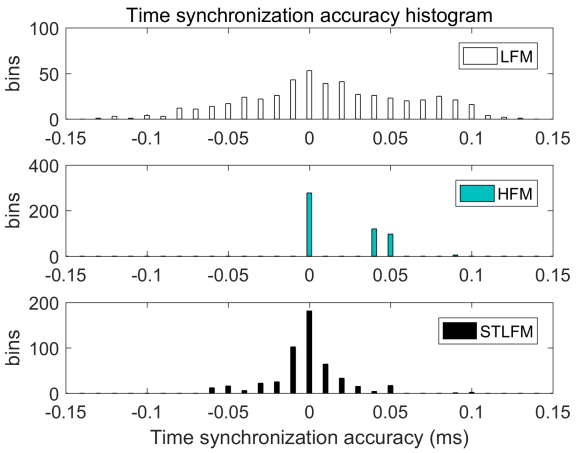

FIGURE 19. Synchronization Error Histogram, SNR = 0 dB.

multi-path components are also shown as severely attenuated, which do not affect the detection of the peaks. White Gaussian Noise (SNR was set to 0 dB, -5 dB, -10 dB) is further superimposed to the experimental channel.

Figure 19 shows the histogram of the simulation results at SNR = -10 dB. It is seen that the STLFM method shows better performance than the LFM signal. In the HFM method, as can be seen, there is still about a half of the errors distributed around 0.04 ms, which means that the multipath component has been captured, and both LFM and STLFM method have better anti-multipath performance than the HFM method.

Figure 20 shows the error distribution probability. It is seen that when the SNR is -10 dB, -5 dB and 0 dB, the performance of the STLFM method does not change much. As the SNR decreases, the performance of the LFM synchronization method also decreases. Specifically, when the SNR decreases from -5 dB to -10 dB, the performance decreases significantly, corresponding to the Figure 12. The adjustment

This article has been accepted for publication in a future issue of this journal, but has not been fully edited. Content may change prior to final publication. Citation information: DOI 10.1109/ACCESS.2019.2901357, IEEE Access

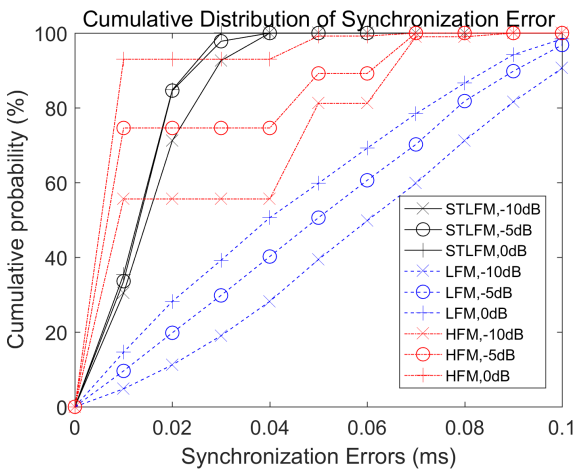

FIGURE 20. Error distribution probability.

of the threshold mentioned in Section IV-A (where $k = 40$ according to the actual conditions) makes the proposed method more adaptable to the degradation of the channel than the LFM method which simply relies on an absolute threshold decision. The accuracy of the HFM algorithm is very high, but due to poor anti-multipath performance, the overall performance is degraded.

TABLE 4. Error mean and MSE over the test channel

Sychronization method	SNR	Error mean (ms)	MSE (ms^2)
STLFM	0 dB	0.01829	4.7×10^{-5}
	-5 dB	0.01860	5.8×10^{-5}
	-10 dB	0.02064	7.9×10^{-5}
LFM	0 dB	0.05633	4.7×10^{-4}
	-5 dB	0.05956	6.9×10^{-4}
	-10 dB	0.06217	7.7×10^{-4}
HFM	0 dB	0.00312	1.1×10^{-4}
	-5 dB	0.01134	4.8×10^{-4}
	-10 dB	0.02273	1.1×10^{-3}

Table 4 shows the statistical results in error mean and MSE by comparing the three methods. The error mean of the proposed method is three times lower than that of the LFM synchronization, and the MSE of the proposed method is about ten times lower than that from the LFM algorithm. Compared with the HFM algorithm, although the proposed method has a slight disadvantage in the error mean, the poor anti-multipath performance of the HFM method results in a large MSE, especially under the low SNR condition.

From the experimental results, we can see that the proposed synchronization algorithm does not keep the synchronization errors in the range of 0.02 ms, which is because the first path to the receiver is considered as the maximum path. The synchronization error of the proposed method is within the range of 0.05 ms at the three SNRs, while the LFM synchronization algorithm barely reaches 90% at the range of 0.1 ms, and even if the accuracy of the HFM method is very high, due to its poor anti-multipath performance, almost a half errors reach 0.04 ms. When the condition of the UWA channel becomes worse, the performance gap between the three methods becomes more pronounced. Compared to the ideal multi-path channel in Section V-A, the actual UWA channel in the experiment is characterized by more complicated multi-path, high noise level, and severe Doppler effect. The proposed method uses adaptive thresholds to deal with the noise, and the correction of symmetry axis is used to correct the Doppler shift, making the performance of the proposed method better than that of the LFM and HFM synchronization method. In summary, the proposed method has higher precision and anti-Doppler performance than the LFM method. Compared with the more accurate HFM method, the proposed method and the LFM method have better anti-multipath performance.

VI. CONCLUSION

In this work, we proposed an adaptive synchronization method for UAC systems and investigated the effectiveness of it using simulation and experimental results. The proposed method utilizes the relative relationship between the two peaks of STLFM signal in the FrFT domain rather than the absolute peak of the LFM signal, which makes it more robust in the synchronization detection compared to traditional LFM synchronization method, and have a better anti-multipath performance than the HFM method, which is more pronounced under low SNR conditions. Statistical results from simulation and experiment show that the proposed synchronization method performs three times lower in the detection error, and five to ten times lower in the MSE compared to the LFM method. These results, including the histogram and the error distribution probability, also make us confidential of the accuracy and stability of the proposed synchronization method used in UAC systems.

REFERENCES

[1] M. Chitre, S. Shahabudeen, and M. Stojanovic, "Underwater acoustic communications and networking: Recent advances and future challenges," Marine Technology Society Journal, vol. 42, no. 1, pp. 103–116, 2008.

[2] J. Li, Y. V. Zakharov, and B. Henson, "Multibranch Autocorrelation Method for Doppler Estimation in Underwater Acoustic Channels," IEEE Journal of Oceanic Engineering, vol. 99, no. 1, pp. 1–15, 2017.

[3] J. Li and Y. V. Zakharov, "Efficient use of space-time clustering for underwater acoustic communications," IEEE Journal of Oceanic Engineering, vol. 43, no. 1, pp. 173–183, 2018.

[4] Y. Zhang, Y. V. Zakharov, and J. Li, "Soft-Decision-Driven Sparse Channel Estimation and Turbo Equalization for MIMO Underwater Acoustic Communications," IEEE Access, vol. 6, pp. 4955–4973, 2018.

[5] Y. Buchris and A. Amar, "A statistical-based Doppler-tolerant criterion for underwater acoustic time synchronization," in OCEANS 2012-Hampton Roads. IEEE, 2012, pp. 1–10.

[6] S. F. Mason, C. R. Berger, S. Zhou, and P. Willett, "Detection, synchronization, and Doppler scale estimation with multicarrier waveforms in underwater acoustic communication," IEEE Journal on Selected Areas in Communications, vol. 26, no. 9, 2008.

[7] G. Zhang, J. M. Hovem, H. Dong, S. Zhou, and S. Du, "An efficient spread spectrum pulse position modulation scheme for point-to-point underwater acoustic communication," Applied Acoustics, vol. 71, no. 1, pp. 11–16, 2010.

[8] Z. X. Sun, Y. Yang, Z. Feng, S. Z. Liu, and Q. Gang, "Underwater acoustic synchronization telemetry research based on binary offset carrier

modulated signal with zero correlation window," Acta Physica Sinica, vol. 63, no. 10, pp. 104 301–104 301, 2014.

[9] A. Jamshidi, "Direct sequence spread spectrum point-to-point communication scheme in underwater acoustic sparse channels," IET communications, vol. 5, no. 4, pp. 456–466, 2011.

[10] C. He, S. Huo, H. Wang, Q. Zhang, and J. Huang, "Single carrier with multi-channel time-frequency domain equalization for underwater acoustic communications," in International Conference on Acoustics, Speech and Signal Processing (ICASSP). IEEE, 2015, pp. 3009–3013.

[11] X. Shu, J. Wang, H. Wang, and X. Yang, "Chaotic direct sequence spread spectrum for secure underwater acoustic communication," Applied Acoustics, vol. 104, pp. 57–66, 2016.

[12] H. Yan, S. Zhou, Z. J. Shi, and B. Li, "A DSP implementation of OFDM acoustic modem," in Proceedings of the second workshop on Underwater networks. ACM, 2007, pp. 89–92.

[13] Z. Jiang, "Detecting of Synchronization Signal for Underwater Acoustic Communication Based on FPGA," in Proceedings of the 2012 International Conference on Electronics, Communications and Control. IEEE Computer Society, 2012, pp. 1420–1422.

[14] F. Wei, X. Xiaomei, Z. Lan, and C. Yougan, "A frame synchronization method for underwater acoustic communication on mobile platform," in International Conference on Image Analysis and Signal Processing (IASP). IEEE, 2010, pp. 518–522.

[15] K. Wang, S. Chen, C. Liu, Y. Liu, and Y. Xu, "Doppler estimation and timing synchronization of underwater acoustic communication based on hyperbolic frequency modulation signal," in International Conference on Networking, Sensing and Control. IEEE, 2015, pp. 75–80.

[16] Q. Zhang, Q. Y. Liu, X. J. Liang, and Y. X. Sun, "Multi-target parameter estimation based on velocity compensation in fmcw radar," in IET International Radar Conference 2015. IET, 2015, pp. 4 .–4 .

[17] T. Jiang, Y. Zhao, and K. Yang, "New method for detection and parameter estimation of stlfm signal," in IET International Radar Conference 2013. IET, 2013, pp. 1–7.

[18] F. Liu, "Detection and parameter estimation of symmetrical triangular LFMCW signal based on fractional Fourier transform," Journal of Electronics and Information Technology, vol. 33, no. 8, pp. 1864–1870, 2011.

[19] J. C. Zheng, W. Xu, J. Guo, and W. D. Xie, "Joint Estimation with Time Delay and Doppler Frequency Shift in the Multi-Carrier Acoustic Communication," in Applied Mechanics and Materials, vol. 263. Trans Tech Publ, 2013, pp. 994–999.

[20] B. S. Sharif, J. Neasham, O. R. Hinton, and A. E. Adams, "A computationally efficient Doppler compensation system for underwater acoustic communications," IEEE Journal of Oceanic Engineering, vol. 25, no. 1, pp. 52–61, 2000.

[21] K. Choi, K. Cheun, and T. Jung, "Adaptive PN code acquisition using instantaneous power-scaled detection threshold under Rayleigh fading and pulsed Gaussian noise jamming," IEEE Transactions on Communications, vol. 50, no. 8, pp. 1232–1235, 2002.

[22] J. Li, L. Liao, and Y. V. Zakharov, "Space-time cluster combining for UWA communications," in OCEANS 2016-Shanghai. IEEE, 2016, pp. 1–6.

[23] J. Li, "DOA tracking in time-varying underwater acoustic communication channels," in OCEANS 2017-Aberdeen. IEEE, 2017, pp. 1–9.

[24] Y. Zakharov and J. Li, "Autocorrelation method for estimation of Doppler parameters in fast-varying underwater acoustic channels," in Underwater Acoustics Conference and Exhibition, Crete, Greece, 2015, pp. 1–4.

[25] W. Niczyporuk, "LFM radar signal detection in the joint time-frequency domain," in Signal Processing Algorithms, Architectures, Arrangements and Applications. IEEE, 2007, pp. 33–37.

[26] Z. Jianhong and Y. Jianyu, "LFM extended target echoes detecting using Radon-Wigner Method," in International Conference on Microwave and Millimeter Wave Technology. IEEE, 2007, pp. 1–4.

[27] R. Wang, J. Huang, T. Ma, and Q. Zhang, "Improved space time prewhitener for linear frequency modulation reverberation using fractional Fourier transform," Journal of the Acoustical Society of America, vol. 128, no. 6, pp. EL361–EL365, 2010.

[28] X. Wang, M. Fei, and X. Li, "Performance of chirp spread spectrum in wireless communication systems," in IEEE Singapore International Conference on Communication Systems, 2008, pp. 466–469.

[29] Y. Chen, L. Guo, and Z. Gong, "The concise fractional Fourier transform and its application in detection and parameter estimation of the linear frequency-modulated signal," Chinese Journal of Acoustics, vol. 36, pp. 70–86, 2017.

[30] C. Liu, H. Pang, and N. Cao, "Research on Time Synchronization Technology of Wireless Sensor Network," in International Conference on Cyber-Enabled Distributed Computing and Knowledge Discovery. IEEE, 2018, pp. 391–394.

[31] F. Yuan, Q. Wei, and E. Cheng, "Joint virtual time reversal communications with an orthogonal chirp spread spectrum over underwater acoustic channel," Applied Acoustics, vol. 117, pp. 122–131, 2017.

[32] G. Yu, S. Piao, and X. Han, "Fractional Fourier transform-based detection and delay time estimation of moving target in strong reverberation environment," IET Radar, Sonar and Navigation, vol. 11, no. 9, pp. 1367–1372, 2017.

[33] J. Zheng, H. Sun, C. Yang, and J. Liu, "A joint synchronization parameter estimation in fractional Fourier transform orthogonal frequency division multiplexing underwater acoustic communication system," Advances in Mechanical Engineering, vol. 8, no. 3, pp. 1–7, 2016.

[34] Y. Deng, F. Yuan, E. Cheng, J. Yi, and Y. Li, "A Synchronization Detection and Time Delay Estimation Algorithm Based on Fractional Fourier Transform," in China Conference on Wireless Sensor Networks. Springer, 2017, pp. 201–210.

[35] Y. Zhao, Y. Hua, W. Gang, J. I. Fei, and F. Chen, "Parameter estimation of wideband underwater acoustic multipath channels based on fractional fourier transform," IEEE Transactions on Signal Processing, vol. 64, no. 20, pp. 5396–5408, 2016.

[36] M.-S. Kim, T. Im, Y.-H. Cho, K. Kim, and H.-L. Ko, "Hfm design for timing synchronization in underwater communications systems," in OCEANS 2017-Aberdeen, 06 2017, pp. 1–4.

[37] M. B. Porter, "The bellhop manual and user's guide: Preliminary draft," Heat, Light, and Sound Research, Inc., La Jolla, CA, USA, Tech. Rep, 2011.

FEI YUAN received the B.S., M.S. and Ph.D. degrees in electronic engineering from Xiamen University, Xiamen, China in 2002, 2005 and 2008, respectively. Now he is an associate professor and supervisor for master in Xiamen University.

He is the member of China Institute of Communications, the Acoustical Society of China, IEEE and IET. He is the reviewer for Journal of Xiamen University, Chinese Journal of Acoustics, Chinese Journal of Scientific Instrument, Applied Acoustic, IJNAOE, etc. He is also the review of provincial and state projects like Natural Science Foundation of China (NSFC), scientific planning subjects of Xiamen, etc. Prof. Yuan's main research interests include underwater acoustic communication, marine information, image processing and embedded system.

ZHENYU JIA received his B. Sc. degree in 2015 from Ocean University of China; Now, he is a Master 's degree candidate in Xiamen University. His main research is underwater acoustic communication.

This article has been accepted for publication in a future issue of this journal, but has not been fully edited. Content may change prior to final publication. Citation information: DOI 10.1109/ACCESS.2019.2901357, IEEE Access

JIANGHUI LI received the B.S. degree in communications engineering from Huazhong University of Science and Technology, Wuhan, China in 2011, the M.Sc. degree in communications engineering, and the Ph.D. degree with receiving the K. M. Stott Prize for excellent research in electronics engineering from the University of York, U.K., in 2013 and 2017, respectively. He has been the first researcher receiving the IEEE OES scholarship in U.K.

From 2011 to 2012, he served as a Research Assistant with the Chinese Academy of Sciences, Beijing, China. Since 2017, he has been a Research Fellow with the University of Southampton, U.K. His current research interests include adaptive signal processing, wireless communications, underwater acoustics, and ocean engineering.

EN CHENG received the B.S., M.S. and Ph.D. degrees in electronic engineering from Xiamen University, Xiamen, China in 1985, 1988 and 2006, respectively. Now he is a professor and supervisor for Ph.D. candidates in Xiamen University.

From 2003 to 2012, he was the department head of the department of communication engineering, Xiamen University, China. And he is the standing deputy director of the Key Laboratory of Underwater Acoustic Communication and Marine Information Technology (Xiamen University), Ministry of Education, Xiamen, China. Since 2002, Prof. Cheng has taken charge of four projects supported by National Natural Science Foundation of China (NSFC), and participated in three projects supported by NSFC. He has published more than 50 papers in international journals and conferences. Prof. Cheng's main research interests include underwater acoustic communication and networks.